Economic Geology
Vol. 95, 2000, pp. 41–48

A Brittle Failure Mode Plot Defining Conditions for High-Flux Flow

Richard H. Sibson†

Department of Geology, University of Otago, P.O. Box 56, Dunedin, New Zealand

Abstract

Stress and fluid-pressure conditions for the initial formation within intact rock of faults (shear fractures), extension fractures, and extensional shears, and for the reshear of existing faults, may all be represented on a generic failure plot of differential stress ($\sigma_1 - \sigma_3$) versus least effective compressive stress, $\sigma_3' = (\sigma_3 - P_f)$, scaled to nominal tensile strength, T (~ half the cohesive strength). Plots of this kind may be used to define maximum sustainable overpressure in different tectonic environments and the structural conditions under which the flow of large fluid volumes may occur through fault-fracture meshes containing gaping extension and extensional shear fractures. They may also be adapted to different tectonic regimes and correlated to depth for particular fluid-pressure conditions. High-flux flow through distributed fault-fracture meshes requires the tensile overpressure condition, $\sigma_3' < 0$, to be met (generally involving $P_f > \sigma_3$), which can only be achieved in the absence of throughgoing cohesionless faults that are well oriented for frictional reactivation in the prevailing stress field. High-flux flow through distributed fault-fracture meshes, intrinsically a transient, pulsing phenomenon, may therefore occur as follows: (1) in effectively intact low-pemeability crust devoid of throughgoing favorably oriented faults, (2) where existing faults have become severely misoriented in the prevailing stress field, and (3) where existing faults have regained cohesive strength through hydrothermal cementation.

Introduction

Hydrothermal mineral deposits are the product of focused flow of large fluid volumes (e.g., Henley, 1985). While structural control in the form of a fault-fracture system is evident for most deposits hosted in low-permeability rocks, it is notable that the hosting faults are generally comparatively low displacement features (Newhouse, 1940; McKinstry, 1948). Within both epizonal and mesozonal systems, hydrothermal veins occupy a mixture of low displacement faults (shear fractures), extension fractures, and extensional shears often interlinked within a mesh structure (Sibson and Scott, 1998; Fig. 1). Vein textures frequently record a history of incremental infilling (e.g., Boullier and Robert, 1992) and show that the extensional shears and extension fractures, in particular, were actively gaping and part of a high-permeability flow system during mineralization. Solubility criteria, incremental vein textures indicating open-space filling, and the need for rapid transport between different P-T-X environments to promote instability and localized precipitation suggest that many hydrothermal deposits result from multiple episodes of rapid, large volume flow. The physical conditions under which such high-permeability flow systems may develop and be sustained are, therefore, crucial to understanding the formation and localization of hydrothermal ore deposits.

Failure Criteria

Fluid pressure, P_f, affects all three macroscopic modes of brittle failure (faults, extension fractures, and extensional shear fractures) through the principle of effective stress. For a fluid-saturated rock mass under triaxial load, effective principal compressive stresses (Terzaghi, 1945; Hubbert and Rubey, 1959) are the following:

$$\sigma_1' = (\sigma_1 - P_f) > \sigma_2' = (\sigma_2 - P_f) > \sigma_3' = (\sigma_3 - P_f). \quad (1)$$

At depth, z, in the crust, fluid-pressure level is conveniently defined in relation to the vertical stress, σ_v, by means of the pore-fluid factor:

$$\lambda_v = \frac{P_f}{\sigma_v} = \frac{P_f}{\rho g z}, \quad (2)$$

where ρ is average rock density and g is gravitational acceleration. Hydrostatic fluid pressure (where fluid-saturated pore space, cracks, and fractures are interconnected through to a water table at the earth's surface) is, therefore, represented by $\lambda_v \sim 0.4$. Overpressured fluids have $\lambda_v > 0.4$ with lithostatic conditions obtaining when fluid pressure equals the vertical stress ($\lambda_v = 1.0$).

Brittle failure conditions for intact isotropic rock may be represented on a Mohr diagram of shear stress, τ, versus effective normal stress, $\sigma_n' = (\sigma_n - P_f)$, by means of a composite failure envelope normalized to nominal tensile strength, T, that is approximately half the cohesive strength, C (the positive intercept of the failure envelope on the τ-axis; Fig. 2). Whereas modern fracture mechanics (e.g., Atkinson, 1987) suggest that tensile rock strength is generally time dependent and depends critically on the size distribution of flaws in the rock mass (accounting for the irreproducibility of tensile strength determinations in the laboratory), nominal tensile strength is retained as a simple means of characterizing comparative rock strength (cf. Lockner, 1995), also serving as a crude measure of relative competence. Note, though, that this classical rock mechanics approach can only be regarded as semiquantitative at best.

The composite failure envelope is constructed by merging the macroscopic Griffith criterion of parabolic form:

$$\tau^2 = 4\sigma_n'T + 4T^2, \quad (3)$$

in the tensile field with the linear Coulomb criterion:

$$\tau = C + \mu_i\sigma_n' = C + \mu_i(\sigma_n - P_f), \quad (4)$$

† Email, rick.sibson@stonebow.otago.ac.nz

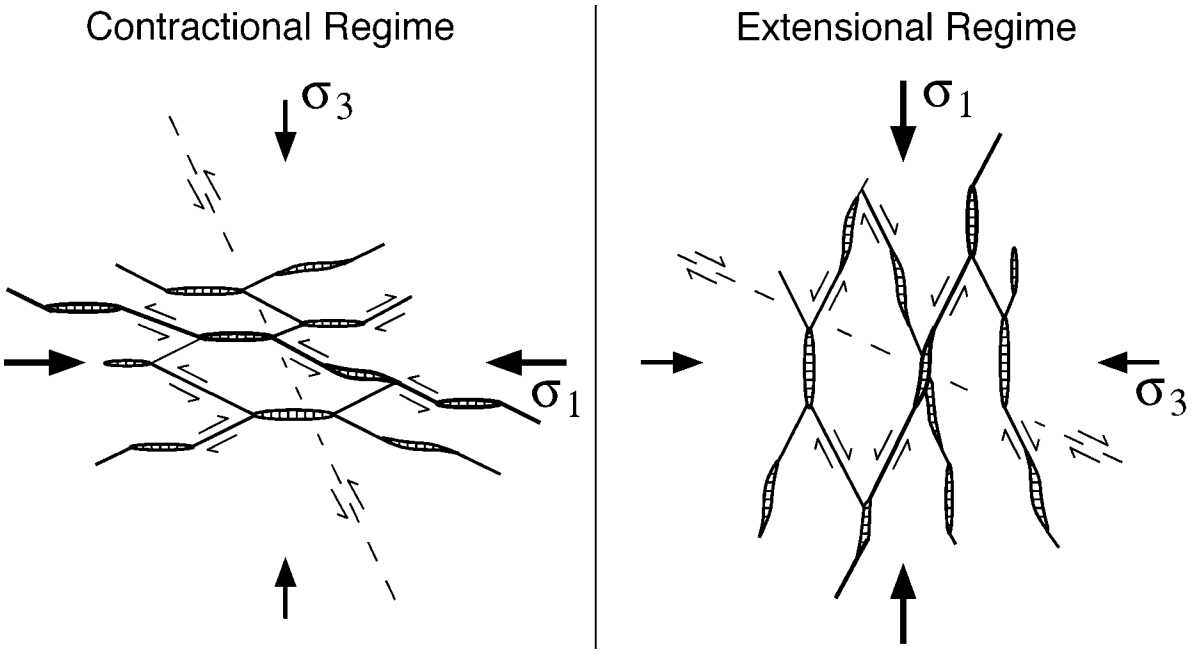

FIG. 1. Fault-fracture meshes in contractional and extensional tectonic regimes (after Hill, 1977). Cross-hatching denotes extension and extensional shear veins; bolder lines indicate eventual amalgamation into throughgoing faults. Dashed lines indicate possible association with faults that are severely misoriented for frictional reactivation in the prevailing stress field.

for compressional shear failure of a rock mass with cohesive shear strength, C, and coefficient of internal friction, μ_i (Brace, 1960; Secor, 1965). The generic failure envelope portrayed in Figure 2 has been constructed by adopting a representative average value for internal friction, $\mu_i = 0.75$, for the Coulomb criterion from the compilation of Jaeger and Cook (1979). This merges with the Griffith criterion in (σ_n', τ) space at the point (0.777T, 2.666T) with C = 2.083T, satisfying the empirical observation that C ~ 2T. At high effective normal stress, empirical failure envelopes also tend to depart from linearity and curve toward parallelism with the σ_n' axis. However, no further account is taken of this nonlinearity because the principal focus of this paper is brittle rock failure at low effective stress.

Three different modes of brittle failure of intact rock may then be recognized (Jaeger and Cook, 1979) and each of the associated failure criteria may be rewritten in terms of the effective principal stresses at failure and the rock tensile strength. Provided $(\sigma_1 - \sigma_3) < 4T$, pure extension fractures form in planes perpendicular to σ_3 for critical stress states represented by circles touching the failure envelope uniquely at the point (-T, 0) such that:

$$\sigma_3' = -T \quad \text{or} \quad P_f = \sigma_3 + T, \tag{5}$$

the criterion for hydraulic extension fracturing.

Faults (shear fractures) form by compressional shear failure when a stress circle with $(\sigma_1 - \sigma_3) > 5.66T$ touches the failure envelope in the compressional field $(\sigma_n' > 0)$. For the linear portion of the failure envelope, such faults form along planes containing the σ_2 direction and lying at an angle, $\theta_s = 0.5\tan^{-1}(1/\mu_i)$ to the σ_1 direction (~ 27° for $\mu_i = 0.75$). For $\mu_i = 0.75$ this part of the failure envelope then becomes:

$$(\sigma_1 - \sigma_3) = 8.33T + 3\sigma_3'. \tag{6}$$

Hybrid extensional shear fractures form when a critical stress circle with diameter, $4T < (\sigma_1 - \sigma_3) < 5.66T$, touches the parabolic part of the failure envelope in the tensile field $(\sigma_n' < 0)$. Shear and extensional opening occur across a fracture containing the σ_2 direction and lying at $0 < \theta_{es} < \theta_s$. The macroscopic Griffith criterion (eq. 3) may be rewritten as:

$$(\sigma_1 - \sigma_3)\ 4T + 4\sqrt{(T^2 + T\sigma_3')}. \tag{7}$$

In the case of an existing cohesionless fault with static coefficient of rock friction, μ_s, the criterion for frictional reactivation (reshear) is:

$$\tau = \mu_s\sigma_n' = \mu_s(\sigma_n - P_f) \tag{8}$$

and is also shown in Figure 2. For existing faults whose poles lie in the plane containing σ_1 and σ_3, this expression may be rewritten in terms of the ratio of effective principal stresses as:

$$\frac{\sigma_1'}{\sigma_3'} = \frac{(\sigma_1 - P_f)}{(\sigma_3 - P_f)} = \frac{(1 + \mu_s\cot\theta_r)}{(1 - \mu_s\tan\theta_r)} \tag{9}$$

so that,

$$(\sigma_1 - \sigma_3) = \frac{\mu_s(\tan\theta_r + \cot\theta_r)}{(1 - \mu_s\tan\theta_r)}\,\sigma_3', \tag{10}$$

where θ_r is the reactivation angle between σ_1 and the plane (Sibson, 1985). From extensive laboratory sliding experiments, Byerlee (1978) found μ_s to be largely independent of rock type and confined within the range $0.6 < \mu_s < 0.85$, so for simplicity we adopt $\mu_s = \mu_i = 0.75$ as a fair representation of rock friction. The optimal reactivation angle (for which the stress ratio reaches a positive minimum) then also occurs when $\theta_r = 0.5\tan^{-1}(1/\mu_s) \sim 27°$ with equation 9 reducing to:

$$(\sigma_1 - \sigma_3) = 3\sigma_3'. \tag{11}$$

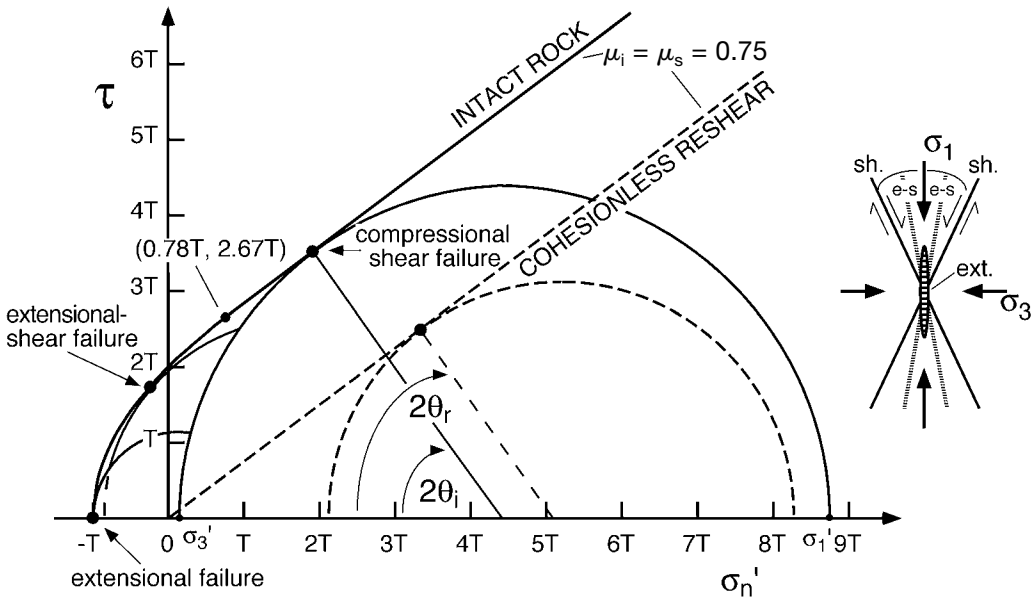

FIG. 2. Composite failure envelope for intact rock (bold line) plus the reshear condition for a cohesionless fault (dashed) plotted on a Mohr diagram of shear stress, τ, against effective normal stress, σ_n', normalized to tensile strength, T. Critical stress circles are shown for the three macroscopic modes of brittle failure and for the reshear of an optimally oriented cohesionless fault (dashed). Expected orientations with respect to the principal stress axes of new-formed shear (sh.), extensional shear (e-s), and extension fractures (ext.) are shown in the attached cartoon.

Generic Failure Mode Plot

Stress conditions for the different brittle failure modes and for reshear may be transcribed (by means of eqs. 5, 6, 7, and 10) to a plot of differential stress, $(\sigma_1 - \sigma_3)$, versus least effective compressive stress, σ_3' (Fig. 3). This offers some advantages for interpreting the stress state at failure in terms of depth and fluid-pressure conditions in different tectonic regimes and also makes clearer the effect of varying tensile strength in a heterogeneous rock mass and the effects of unfavorably oriented existing faults that contain the σ_2 axis. In a sense, it may be viewed as a generic failure mode plot scaled to tensile strength, T, given the representative values of μ_s and μ_i used in its construction. Note, however, that the construction can be readily adapted for different values of these critical material parameters.

For most sedimentary rocks, $1 < T < 10$ MPa, but crystalline rocks may have long-term tensile strengths of 20 MPa or more (Lockner, 1995). In Figure 3, composite failure curves for intact rock with varying tensile strength ($T < 20$ MPa) are plotted as bold continuous lines with the fields of different failure modes defined by shading differences. The bold dashed line is the reshear condition for an existing cohesionless fault containing the σ_2 direction that is optimally oriented (at ~ 27° to σ_1) for frictional reactivation; thin dashed lines represent the reshear conditions for nonoptimally oriented cohesionless faults.

Consider first the failure conditions for intact rock. Only compressional shear failure is possible with $\sigma_3' = (\sigma_3 - P_f) > 0$. Formation of extension fractures and/or extensional shears requires the tensile overpressure condition, $\sigma_3' = (\sigma_3 - P_f) < 0$, to be met, in turn requiring either $\sigma_3 < 0$ or $P_f > \sigma_3$. Note that these failure fields become larger with increased tensile strength so that mixed mode failure becomes likely in a rock mass where tensile strength varies. It is in these circumstances ($\sigma_3' < 0$ within a heterogeneous rock mass) that mesh structures comprising interlinked shear, extensional, and extensional shear fractures distributed throughout a substantial rock volume may be self-generated by migrating fluids to form conduits for high-flux flow (Sibson, 1996).

The optimal reshear condition demonstrates again the buffering effect (against brittle failure of intact rock) of an existing cohesionless fault that is favorably oriented for frictional reactivation. However, as the orientation of an existing fault becomes progressively less favorable (greater or less than optimal), the reshear condition intercepts the failure envelopes for brittle failure of intact rock. For particular values of tensile strength and fault orientation there exist critical σ_3' values, below which reshear will occur in preference to new compressional shear failure and above which the reverse is the case. Reactivation of existing cohesionless faults oriented at up to twice the optimal orientation (i.e., $\theta_r <$ ca. 54°) prevents attainment of the tensile overpressure condition, $\sigma_3' < 0$, and it is not until $\theta_r >$ ca. 60° (severe misorientation) that the conditions for extensional shear or pure extension fracturing can be achieved. Cohesionless faults other than those containing the σ_2 direction may likewise inhibit brittle failure of intact rock, but the critical fault orientations in 3-D then depend strongly on the value of the intermediate principal stress.

Different tectonic regimes

The general failure mode plot (Fig. 3) can be readily modified to plots of differential stress $(\sigma_1 - \sigma_3)$ versus effective vertical stress, $\sigma_v' = (\sigma_v - P_f)$, for uniform Andersonian stress

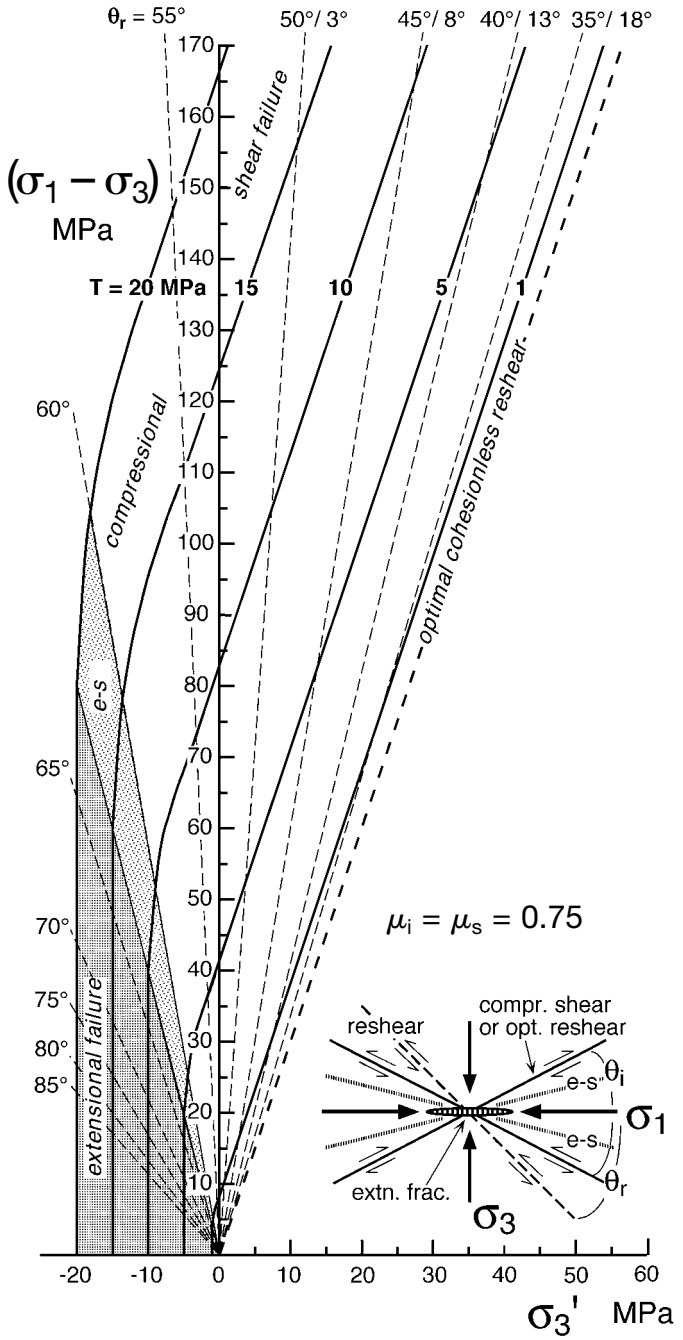

FIG. 3. Generic failure plot of differential stress, $(\sigma_1 - \sigma_3)$, against effective least principal stress, σ_3'. Bold lines represent failure condition for intact rock at various tensile strengths with the fields of pure extension fracturing and extensional shear fracturing shaded. Bold dashed line is the reshear condition for a cohesionless fault containing the σ_2 direction that is optimally oriented for frictional reactivation ($\theta_r \sim 27°$); thin dashed lines represent the reshear conditions for nonoptimally oriented cohesionless faults oriented at varying θ_r to the σ_1 direction.

regimes with one of the principal stresses vertical (see Sibson, 1998). Brittle failure mode plots for optimal reshear and for intact rock with T = 10 and 20 MPa are plotted in Figure 4 for contractional ($\sigma_v = \sigma_3$) and extensional ($\sigma_v = \sigma_1$) tectonic regimes. These two plots also represent the end-member cases for strike-slip faulting ($\sigma_3 \le \sigma_v = \sigma_2 \le \sigma_1$). Values of σ_v' equate to depth for different pore-fluid factors, λ_v.

Note first the relative ease, in terms of differential stress and/or fluid pressure level, of deforming a rock mass by brittle fracturing and faulting in an extensional as opposed to a contractional regime. Second, for intact rock with tensile strength, T, there is a general progression with increasing σ_v' from extensional fracturing through extensional shear to compressional shear failure. Most importantly, however, for positive σ_v' ($\lambda_v < 1.0$) only compressional shear failure can occur in contractional tectonic regimes, whereas extensional and extensional shear fractures may form in extensional regimes to depths dependent on rock tensile strength.

Maximum Sustainable Overpressure

Formation (or reactivation) of fractures and faults in low-permeability rocks provides flow conduits limiting the degree of overpressuring. A critical issue, therefore, is the lowest σ_3' (corresponding to the highest P_f and λ_v values) that can be sustained in different tectonic environments. Two end-member situations are of special interest. Hydraulic extension fracturing occurs at the lowest σ_3' value for a given tensile strength but requires $(\sigma_1 - \sigma_3) < 4T$. If, on the other hand, fluid overpressure is buffered by the presence of throughgoing cohesionless faults that are optimally oriented for reactivation, then maximum sustainable overpressure is governed by equation 11 and diminishes with increasing differential stress. Barton et al. (1995) found, for example, that the most permeable fracture systems in crystalline rocks tend to be those that are optimally oriented for reshear in the prevailing stress field.

The two situations are illustrated in Figure 5 where maximum sustainable λ_v is plotted against depth for a thrust fault regime ($\sigma_v = \sigma_3$) and for a normal fault regime ($\sigma_v = \sigma_1$) again representing the end-member cases for strike-slip faulting. Following Secor (1965), λ_v values for hydraulic extension fracturing at maximum permissible levels of differential stress ($(\sigma_1 - \sigma_3) = 4T$) are plotted against depth for different values of T in the two regimes. Also shown (from eq. 11) are the λ_v values required at different levels of differential stress for reshear of optimally oriented cohesionless faults in each regime. Intermediate situations between these end members arise when the faults retain some degree of cohesive strength.

The presence of throughgoing cohesionless faults drastically lowers the maximum fluid overpressure that can be sustained at a particular depth and the higher the differential stress, the lower the sustainable overpressure. Well-oriented throughgoing faults lacking cohesive strength therefore limit the amplitude of any fluid-pressure cycling that may accompany fault valve action in overpressured crust, lowering the potential for hydrothermal precipitation from drops in fluid pressure.

Conditions for High-Flux Flow

Rock permeability generally increases as $P_f \rightarrow \sigma_3$ and σ_3' decreases (Seront et al., 1998), increasing flow rate for a given head gradient. In low-permeability rock masses, however, bulk permeability is dominated by fracture flow and flow rate becomes highly sensitive to fracture aperture, varying as the cube of aperture for a set of parallel planar fractures (Snow,

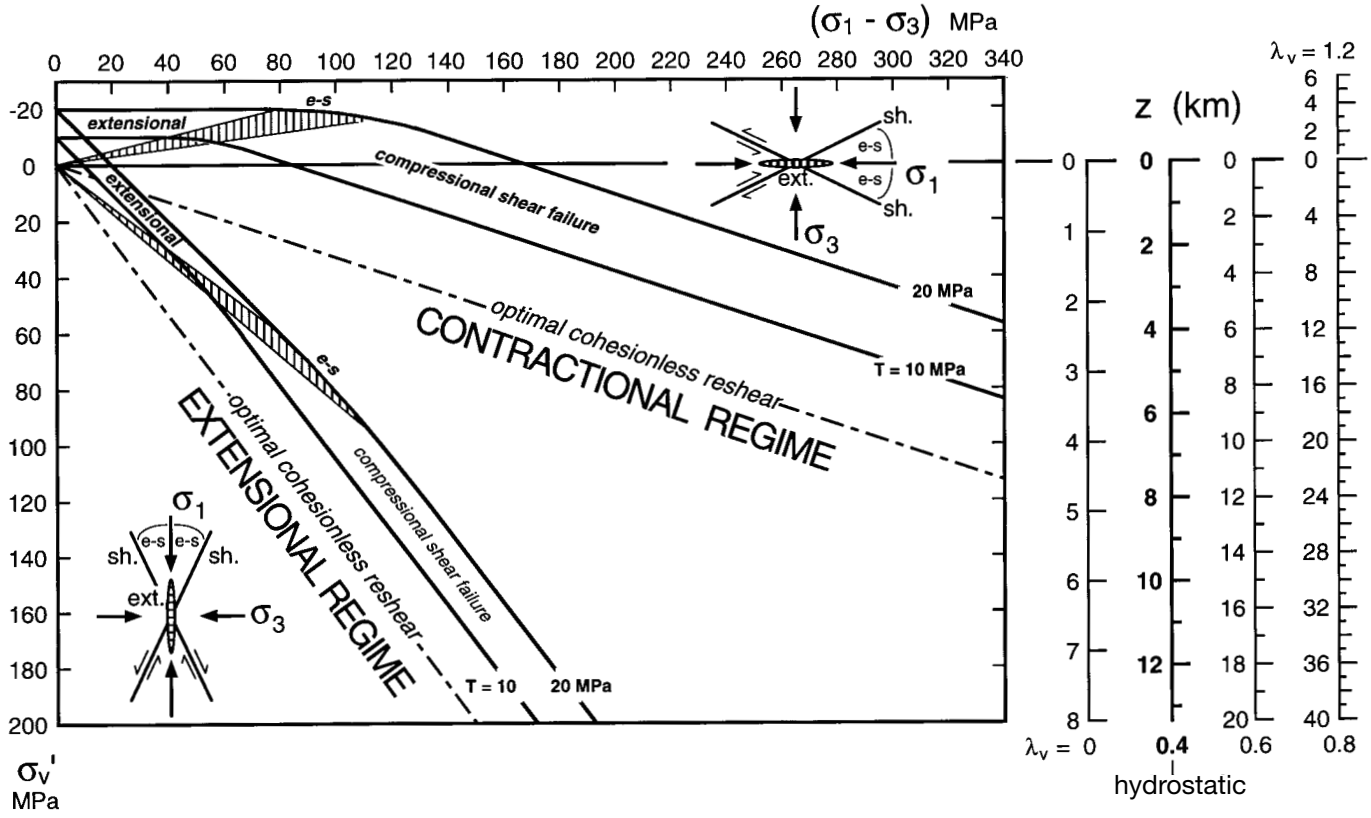

FIG. 4. Brittle failure mode plots with differential stress plotted against effective vertical stress, σ_v', for contractional ($\sigma_v = \sigma_3$) and extensional ($\sigma_v = \sigma_1$) tectonic regimes. Dashed lines represent the optimal reshear conditions for cohesionless faults, solid lines the brittle failure curves for intact rock with the different failure fields outlined. Insets show expected orientations of the resulting brittle structures. Effective vertical stress can be equated to depth (right) for different values of the pore-fluid factor, λ_v.

1968). Thus while faults may significantly enhance bulk permeability, especially postfailure, maximum flow rates will be achieved at the highest levels of fluid overpressure with gaping extensional and extensional shear fractures distributed throughout a rock volume. This requires the tensile overpressure condition, $\sigma_3' < 0$, to be maintained, at least locally, providing a general condition for high-flux flow in low-permeability rocks.

Note from Figure 3 that the higher the tensile strength, the greater the range of differential stress levels under which extensional and extensional shear failure may occur in preference to faulting. High-flux flow is, therefore, favored by the presence of high tensile strength material within the rock mass, with fault-fracture meshes forming in material of varying tensile strength provided the tensile overpressure condition is met for the stronger material. Maintaining gaping extensional and extensional shear fractures within a fault-fracture mesh, therefore requires either absolute tensile values of σ_3 or the condition $P_f > \sigma_3$ to obtain locally. Local reductions in σ_3 may be brought about by stress field heterogeneity, for example at fault tips or in dilational jogs between en echelon fault segments (Segall and Pollard, 1980).

Attainment of the tensile overpressure condition allowing activation of fault-fracture meshes is prevented by the presence of throughgoing cohesionless faults that are well oriented for frictional reactivation (Figs. 2 and 3). Indeed, field evidence suggests that distributed fault-fracture meshes are in many cases precursors to the development of throughgoing faults which form by the progressive amalgamation of mesh components into a favorably oriented structure, after which the rest of the mesh system becomes inactive (Sibson and Scott, 1998). Conditions favoring high-flux flow at maximum sustainable overpressure are, therefore, likely to be rather short-lived.

Given this important constraint against the development of extensional and extensional shear fractures in the presence of existing faults, there appear to be three situations where high-flux flow may develop through fault-fracture meshes.

1. Overpressured fluids may lead to mesh development in effectively intact crust devoid of throughgoing faults that are well oriented for frictional reactivation. Such a situation may arise, for example, in crust that has been recently reconstituted through metamorphism (Sibson and Scott, 1998).

2. Mesh development may occur in association with existing faults that have become severely misoriented in the prevailing stress field, perhaps through progressive domino rotation of an existing fault set. It is this circumstance in contractional regimes that leads to the most extreme form of fault-valve action along steep reverse faults, with mesh activation from fluid pressure build-up preceding each episode of reverse fault slip, followed by postfailure high-flux discharge along the faults (Sibson et al., 1988; Cox, 1995).

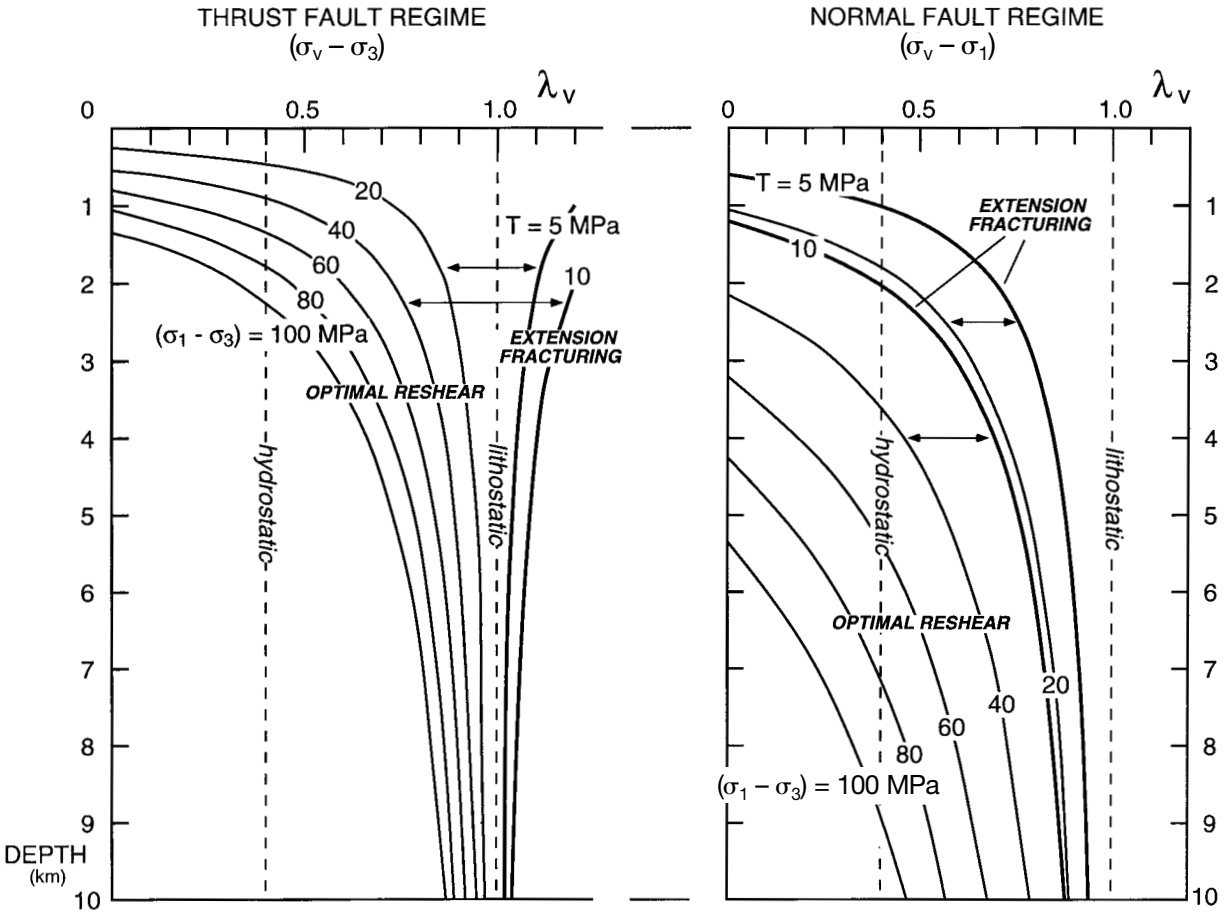

FIG. 5. Maximum sustainable fluid pressures (λ_v) plotted against depth in contractional and extensional tectonic regimes. Bold lines for T = 5 and 10 MPa assume that fluid overpressure is limited by the formation of hydraulic extension fractures under maximum allowable differential stress ($(\sigma_1 - \sigma_3) = 4T$). Thin lines are the maximum sustainable overpressures in the presence of existing, optimally oriented, cohesionless faults under different levels of differential stress. Double-headed arrows link sustainable fluid pressure-curves for the different failure modes at the same differential stress level.

3. Mesh activation may be sustained despite the development of throughgoing, favorably oriented faults when, between successive slip increments, the faults regain cohesive strength by hydrothermal cementation to values approaching intact crust (e.g., Nguyen et al., 1998).

Discussion

It is apparent from Figure 4 that high-flux flow through distributed fault-fracture meshes (perhaps self-generated in the prevailing stress field by fluid migration) may occur under hydrostatic fluid pressures in the near surface of extensional and/or transtensional tectonic settings to depths dependent on maximum rock tensile strength. Stress heterogeneities induced by structural irregularities such as dilational fault jogs may further serve to localize flow in areas of reduced σ_3. It is the coincidence of these shallow, high-flux conduits with the boiling horizons of ascending, near-hydrostatically pressured geothermal plumes (Henley, 1985) that defines the epizonal environment for mineralization. In contrast, development of fault-fracture meshes in contractional and/or transpressional regimes requires fluids overpressured to supralithostatic values ($P_f > \sigma_v$), unless structural irregularities locally create stress heterogeneities with $\sigma_3 < \sigma_v$. The common association in mesozonal lode gold systems of arrays of flat-lying extension veins associated with fault veins on steep, severely misoriented reverse faults provide further examples of mesh conduits acting as channels for episodic large volume flow under supralithostatic levels of fluid pressure (Sibson et al., 1988; Cox, 1995).

Flow through fault-fracture meshes is in general unlikely to be steady state given dynamic local interactions between stress and fluid-pressure cycling, strength variations from cementation, and the creation and destruction of fracture permeability by fracturing and hydrothermal self-sealing. Such complex systems have the potential for a range of burping fault-valve behavior over varying time periods, leading to episodic large volume flow accompanied by high-amplitude fluid-pressure cycling. However, the special conditions allowing high-flux flow are unlikely to be maintained for lengthy time periods as the development of throughgoing, favorably oriented faults will generally curtail such activity. These factors help to account for the old mining adage that hydrothermal deposits of economic significance are generally hosted on comparatively low-displacement fault-fracture systems.

Acknowledgments

Thanks to Graeme Broadbent, Lance Miller, Howard Poulsen, and François Robert who over many years have focused my attention on these issues, and to François Cornet and Stephen Cox for insightful reviews. This work was funded by the New Zealand Public Good Science Fund through Foundation for Research, Science, and Technology (FRST) contract C05611.

March 31, July 9, 1999

REFERENCES

Atkinson, B.K., ed., 1987, Fracture mechanics of rock: London, Academic Press, 534 p.

Barton, C.A., Zoback, M.D., and Moos, D., 1995, Fluid flow along potentially active faults in crystalline rock: Geology, v. 12, p. 683–686.

Boullier, A-M., and Robert, F., 1992, Paleoseismic events recorded in Archean gold-quartz vein networks, Val d'Or, Abitibi, Quebec, Canada: Journal of Structural Geology, v. 14, p. 161–180.

Brace, W.F., 1960, An extension of the Griffith theory of fracture to rocks: Journal of Geophysical Research, v. 65, p. 3477–3480.

Byerlee, J.D., 1978, Friction of rocks: Pure and Applied Geophysics, v. 116, p. 615–626.

Cox, S.F., 1995, Faulting processes at high fluid pressures: An example from the Wattle Gully fault, Victoria, Australia: Journal of Geophysical Research, v. 100, p. 12,841–12,859.

Henley, R.W., 1985, The geothermal framework of epithermal deposits: Reviews in Economic Geology, v. 2, p. 1–24.

Hill, D.P., 1977, A model for earthquake swarms: Journal of Geophysical Research, v. 82, p. 347–352.

Hubbert, M.K., and Rubey, W.W., 1959, Role of fluid pressure in mechanics of overthrust faulting: Bulletin of the Geological Society of America, v. 70, p. 115–166.

Jaeger, J.C., and Cook, N.G.W., 1979, Fundamentals of rock mechanics, 3rd ed.: London, Chapman and Hall, 593 p.

Lockner, D.A., 1995, Rock failure, *in* Ahrens, T.J., ed., Rock physics and phase relations: A handbook of physical constants: American Geophysical Union Reference Shelf, v. 3, p. 127–147.

McKinstry, H.E., 1948. Mining geology: New Jersey, Prentice-Hall, 677 p.

Newhouse, W.H., 1940, Openings due to movement along a curved or irregular fault plane: Economic Geology, v. 35, p. 444–464.

Nguyen, P.T., Cox, S.F., Harris, L.B., and Powell, C. McA., 1998, Fault-valve behaviour in optimally oriented shear zones: An example at the Revenge gold mine, Kambalda, Western Australia: Journal of Structural Geology, v. 20, p. 1625–1640.

Secor, D.T., 1965, Role of fluid pressure in jointing: American Journal of Science. v. 263, p. 633–646.

Segall, P., and Pollard, D.D., 1980, Mechanics of discontinuous faults: Journal of Geophysical Research, v. 85, p. 4337–4350.

Seront, B., Wong, T-F., Caine, J.S., Forster, C.B., Bruhn, R.L., and Fredrich, J.T., 1998, Laboratory characterization of hydromechanical properties of a seismogenic normal fault system: Journal of Structural Geology, v. 20, p. 865–882.

Sibson, R.H., 1985, A note on fault reactivation: Journal of Structural Geology, v. 7, p. 751–754.

——1996, Structural permeability of fluid-driven fault-fracture meshes: Journal of Structural Geology, v. 18, p. 1031–1042.

——1998, Brittle failure mode plots for compressional and extensional tectonic regimes: Journal of Structural Geology, v. 20, p. 655–660.

Sibson, R.H., and Scott, J., 1998, Stress/fault controls on the containment and release of overpressured fluids: Examples from gold-quartz vein systems in Juneau, Alaska; Victoria, Australia and Otago, New Zealand: Ore Geology Reviews, v. 13, p. 293–306.

Sibson, R.H., Robert, F., and Poulsen, K.H., 1988, High-angle reverse faults, fluid-pressure cycling, and mesothermal gold-quartz deposits: Geology, v. 16, p. 551–555.

Snow, D.T., 1968, Rock fracture spacings, openings, and porosities: Journal of the Soil Mechanics and Foundations Division, American Society of Civil Engineers, Proceedings, v. 94, p. 73–91.

Terzaghi, K. Van, 1945, Stress conditions for the failure of saturated concrete and rock: Proceedings, American Society for Testing Materials, v. 45, p. 777–801.